Polymer 68 (2015) 25–34

Contents lists available at ScienceDirect

Polymer

journal homepage: www.elsevier.com/locate/polymer

Epoxy nanocomposites containing magnetite-carbon nanofibers aligned using a weak magnetic field

Shuying Wu [a], Raj B. Ladani [a], Jin Zhang [b], Anthony J. Kinloch [c], Zhiheng Zhao [d], Jun Ma [d], Xuehua Zhang [e], Adrian P. Mouritz [a], Kamran Ghorbani [f], Chun H. Wang [a, *]

[a] Sir Lawrence Wackett Aerospace Research Centre, School of Aerospace, Mechanical & Manufacturing Engineering, RMIT University, GPO Box 2476, Melbourne, VIC 3001, Australia
[b] Australian Future Fibres Research and Innovation Centre, Institute for Frontier Materials, Deakin University, VIC 3220, Australia
[c] Department of Mechanical Engineering, Imperial College London, London SW7 2BX, UK
[d] School of Advanced Manufacturing and Mechanical Engineering, University of South Australia, SA 5095, Adelaide, Australia
[e] School of Civil, Environmental & Chemical Engineering, RMIT University, GPO Box 2476, Melbourne, VIC 3001, Australia
[f] School of Electrical and Computer Engineering, RMIT University, GPO Box 2476, Melbourne, VIC 3001, Australia

ARTICLE INFO

Article history:
Received 21 March 2015
Received in revised form
25 April 2015
Accepted 29 April 2015
Available online 8 May 2015

Keywords:
Carbon nanofibers
Magnetic field alignment
Epoxy nanocomposites

ABSTRACT

Novel magnetite-carbon nanofiber hybrids (denoted by "Fe_3O_4@CNFs") have been developed by coating carbon nanofibers (CNFs) with magnetite nanoparticles in order to align CNFs in epoxy using a relatively weak magnetic field. Experimental results have shown that a weak magnetic field (~50 mT) can align these newly-developed nanofiber hybrids to form a chain-like structure in the epoxy resin. Upon curing, the epoxy nanocomposites containing the aligned Fe_3O_4@CNFs show (i) greatly improved electrical conductivity in the alignment direction and (ii) significantly higher fracture toughness when the Fe_3O_4@CNFs are aligned normal to the crack surface, compared to the nanocomposites containing randomly-oriented Fe_3O_4@CNFs. The mechanisms underpinning the significant improvements in the fracture toughness have been identified, including interfacial debonding, pull-out, crack bridging and rupture of the Fe_3O_4@CNFs, and plastic void growth in the polymer matrix.

1. Introduction

Many applications of polymeric materials in electronic devices, fuel storage and transportation, automotive, and aerospace products demand good mechanical properties for structural integrity and high electrical conductivities to dissipate static electricity [1]. Carbon nanomaterials, such as carbon nanotubes (CNTs), carbon nanofibers (CNFs), and graphene nanosheets (GNSs), have emerged as promising nanofillers for polymer nanocomposites due to their outstanding mechanical and electrical properties [2–4]. The introduction of carbon nanofillers into polymers can greatly improve their electrical and mechanical properties [4–6]. The enhancements in these properties can be achieved at relatively low loadings, which arises from their high aspect ratio, leading to them frequently being superior fillers compared to the conventional micrometer-sized fillers [7]. However, the property improvements achieved to date using carbon nanofillers are still well below the theoretical predictions due to the difficulty in achieving (i) a uniform dispersion of the nanofillers in the polymer matrices, (ii) appropriate interfacial bonding with the polymer matrices [3,5,8], and more importantly, (iii) alignment of the nanofillers. Indeed, aligned carbon nanofillers have been found to produce more significant improvements in the mechanical and electrical properties, in the direction of the alignment, when compared to their randomly-oriented counterparts [9–13].

Different approaches for aligning carbon nanofillers have been reported in the literature, mainly based on mechanical stretching [14,15] or the application of an electric field [16,17] or magnetic field [18–23]. Although using an electric field is recognized as an effective method, this technique is typically restricted to materials with very low electrical conductivity, since the field strength is usually limited to avoid dielectric breakdown of the polymer [23]. Moreover, due to their low magnetic susceptibility [18–21], an extremely strong magnetic field (e.g. of several Teslas) is usually required to align carbon-based nanofillers. For instance, Camponeschi and co-workers [21] employed a magnetic field of up to 25 T

* Corresponding author. Tel.: +61 3 9925 6115.
E-mail address: chun.wang@rmit.edu.au (C.H. Wang).

http://dx.doi.org/10.1016/j.polymer.2015.04.080

to orient and align CNTs in an epoxy resin and found that the properties of the resulting nanocomposites were superior to those prepared in the absence of a magnetic field. Another similar attempt was reported by Mahfuz and co-workers [20] who used magnetic fields of up to 28 T to align CNFs in a two-phase toughened epoxy resin system and achieved 21% and 3% increases in the compressive strength and modulus compared to randomly-oriented CNFs. The necessity to employ such high magnetic fields limits the practical application of this method. Therefore, various methods have been reported to functionalise carbon nanofillers with magnetic nanoparticles, especially iron-based nanoparticles, so as to align the nanofiller in a polymer matrix without needing to employ high magnetic fields [24–27]. For instance, magnetite (Fe_3O_4) decorated single-walled CNTs have been developed using a sonochemical oxidation process and these hybrid nanofillers were successfully aligned in an epoxy using a relatively weak magnetic field [24]. In addition to CNTs, graphene-based magnetic hybrids have also been prepared by attaching Fe_3O_4 nanoparticles onto the graphene nanoplatelets and/or graphene oxide, using a wet-chemical co-precipitation method. The graphene hybrids were aligned in an epoxy under a relatively low magnetic field to achieve high thermal conductivity [26] and good gas barrier properties [27].

CNFs have a relatively high aspect ratio and are an excellent low-cost alternative to CNTs [28]. However, most of the reported research efforts on functionalising CNFs by magnetic iron oxide nanoparticles have been either based on complex chemical methods or a very high temperature treatment [29,30]. Moreover, to the best of our knowledge, there is no report on aligning iron oxide-CNFs in an epoxy resin using a relatively low magnetic field to selectively reinforce the epoxy polymer in a preferred orientation.

The present work aims to explore the functionalisation process to coat carbon nanofibers with magnetic iron oxide nanoparticles by co-precipitation and to align the resultant nanofiber hybrids in an epoxy resin for developing epoxy nanocomposites with anisotropic electrical and mechanical properties. The functionalised carbon nanofibers, denoted by Fe_3O_4@CNFs, are first dispersed into a liquid epoxy resin which is then cured under a relatively weak magnetic field of ~50 mT. The electrical conductivity and fracture toughness of the cured epoxy nanocomposites, containing either randomly-oriented or aligned Fe_3O_4@CNFs are measured and compared. Finally, the toughening mechanisms are identified from fractographic studies.

2. Experimental details

2.1. Materials

Vapour grown carbon nanofibers (VGCNFs) (Pyrograf®-III, grade PR-24-XT-HHT) used in the present work are fully graphitized at 2800 °C and contain a very low content of catalyst (iron <100 ppm). They therefore possess a relatively high electrical conductivity and a low magnetic susceptibility. According to material data supplied by the manufacturer, the CNFs have an average diameter in the range of 70–200 nm and a length of between 50 and 200 μm. The epoxy resin used is a liquid blend of bisphenol A and bisphenol F ('105' from West System) together with a slow-curing hardener ('206' from West System) which is a blend of aliphatic amines and aliphatic amine adducts based on diethylene triamine and triethylenetetramine. Concentrated nitric acid (70%) was obtained from RCI Labscan. Iron (II) sulfate heptahydrate ($FeSO_4 \cdot 7H_2O$), anhydrous iron chloride, and ammonia hydroxide (NH_4OH) were sourced from Sigma–Aldrich, Australia. Carbon fiber composite substrates were manufactured from T700 carbon fiber/epoxy prepreg (VTM 264) supplied by Advanced Composites Group. Twelve plies of this unidirectional prepreg with dimensions of 300 mm × 250 mm × 2.35 mm were used to fabricate the substrates for the fracture toughness tests by curing the prepreg plies in an autoclave at 120 °C and under a pressure of ~650 kPa for 1 h, as recommended by the supplier.

2.2. Preparation of the magnetic Fe_3O_4@CNFs

To functionalise with Fe_3O_4 nanoparticles, the CNFs were first treated with an oxidative mineral acid. Typically, 2 g of as-received CNFs were initially mixed with 200 mL of concentrated nitric acid under vigorous stirring. This mixture was then treated at 100 °C for 6 h under magnetic stirring. After this treatment, the mixture was washed several times by deionized water until reaching a pH value of ~7. The samples were vacuum filtrated and dried in a vacuum oven. After this acid treatment, the CNFs are expected to possess oxygen-containing functional groups, such as carboxylic, lactone and phenolic quinone, on their surfaces and are denoted by CNFs-OX [31].

The Fe_3O_4 nanoparticles were fabricated by a facile co-precipitation method [32,33] from the CNFs-OX materials, prepared as described above. Firstly, 0.225 g of the CNFs-OX were dispersed in 200 mL distilled water by ultraprobe sonication for 15 min, into which 0.225 g of $FeCl_3$ was added whilst stirring. The mixture was vigorously stirred for 15 min whilst being heated to 50 °C under a nitrogen (N_2) atmosphere. Then, 0.18 g of $FeSO_4 \cdot 7H_2O$ was added, with continuous stirring under a N_2 atmosphere for 30 min. Next, 15 mL of 8 M NH_4OH aqueous solution was added drop-wise to precipitate ferric and ferrous salts. The pH value of the mixture was kept at ~10 and the reaction was carried out at 50 °C for 30 min under vigorous magnetic stirring, and N_2 was continuously purged during the reaction to prevent oxidation. The Fe_3O_4@CNFs hybrids were obtained by magnetic separation, washed with distilled water and ethanol, and finally dried under vacuum at 50 °C.

2.3. Preparation of the bulk epoxy nanocomposites with Fe_3O_4@CNFs

The epoxy nanocomposites containing Fe_3O_4@CNFs were prepared as described below. The Fe_3O_4@CNFs were firstly dispersed in a small amount of acetone by bath sonication for 15 min (the typical concentration being 20 mg/mL). Epoxy resin was then added and the sonication process was continued for 1 h. The acetone was then removed under reduced pressure. Subsequently, a stoichiometric amount of hardener was added and the mixture was poured into a rubber mold for curing. To align the Fe_3O_4@CNFs, the mixture was subjected to a weak magnetic field of ~50 mT generated by a pair of permanent magnets whilst it was being cured. Using a gaussmeter, the intensity of the magnetic field was measured to be approximately 50 mT at a distance of 4 cm between a pair of ferrite magnets which were 150 × 50 × 25.4 mm in size. Initial, exploratory, experiments were carried out using different intensities of magnetic field, ranging from 20 mT to 50 mT by changing the gap between the magnets. Since the alignment of the Fe_3O_4@CNFs needs to be completed prior to gelation of the epoxy (the gel time of the epoxy is around 20–30 min at 25 °C), a magnetic field strength of 50 mT was finally selected so that the Fe_3O_4@CNFs could be highly aligned within approximately 10 min from the application of the magnetic field. Epoxy nanocomposites containing various weight contents (i.e. 0.0, 0.2, 0.4, and 0.6 wt%) of the Fe_3O_4@CNFs were prepared.

2.4. Preparation of composite joints

Prior to the application of the liquid epoxy resin mixture as an adhesive to form bonded joints, the surfaces of the carbon-fiber

composite substrates were sandblasted and thoroughly degreased with acetone. The substrates were then cleaned with distilled water and dried using compressed air. A dam made of silicone rubber was used to prevent the liquid epoxy resin mixture from flowing out and spacers (1 mm thick) were placed between the substrates to control the thickness of the adhesive layer. A sharp pre-crack in the mid-plane of the adhesive layer was pre-formed by using Teflon thin film (50 μm thick). The epoxy resin mixtures containing the 0.0, 0.2, 0.4, and 0.6 wt% of Fe_3O_4@CNFs and the hardener were prepared following the procedure described in Section 2.3 and then poured between the substrates which were subsequently placed between two permanent magnets to induce the alignment (Fig. 1a). The magnetic field direction is perpendicular to the bonding surfaces. The joints were cured at room temperature for 48 h. Once cured, the samples were cut into double-cantilever beam (DCB) specimens with the dimensions shown in Fig. 1b.

2.5. Characterization

2.5.1. Characterization of the Fe_3O_4@CNFs

KBr disks were prepared and dried under vacuum at 80 °C, and the measurement of Fourier transform infrared (FTIR) spectra were conducted using a Bruker Vertex 70 FTIR spectrometer. The spectra were recorded by taking the average of sixty four scans in the wave number range of 400–4000 cm^{-1} at a resolution of 4 cm^{-1}. X-ray diffraction (XRD) patterns of the samples were collected using a Bruker D8 Advance diffractometer with Cu-Kα radiation (λ = 1.54 Å). X-ray photoelectron spectroscopy (XPS) was performed using a Thermo K-alpha XPS instrument at a pressure ~1×10^{-9} Torr with the core levels aligned with the C 1s binding energy of 284.8 eV. The morphology of the samples was investigated using a transmission electron microscope (TEM) JEOL JEM 1010 operating at 100 kV and equipped with a Gatan Orius SC600 CCD camera for digital imaging. TEM samples were prepared by dropping ethanol dispersion of Fe_3O_4@CNFs on carbon-coated copper grids (200 mesh). Scanning electron microscopy (SEM) analysis was performed using a FEI Nova NanoSEM, equipped with an Oxford X-MaxN 20 energy dispersive X-ray (EDX) detector, operating at 15 kV and a 5 mm working distance. Samples were drop cast on a piece of silicon wafer which was then attached to an aluminium SEM stub with double-sided carbon tape.

2.5.2. Characterization of the epoxy nanocomposites

The alignment of the Fe_3O_4@CNFs in the epoxy was investigated using optical microscopy, TEM, and SEM. For the optical microscopy observations, a drop of a mixture of the epoxy resin/Fe_3O_4@CNFs was placed onto a glass slide.

For TEM observations, epoxy nanocomposites were microtomed into ultrathin sections of ~70 nm thick with a diamond knife using a Leica EM ultramicrotome, which were collected on 200 mesh copper grids. For SEM observations, the specimens were cryogenically fractured in liquid nitrogen and then surface-coated with a thin layer of gold prior to observation. The electrical resistivity was measured at room temperature using an Agilent 4339B high-resistivity meter equipped with a 16008B resistivity cell. The samples were tightly screw-pressed between two cylindrical electrodes having a diameter of 26 mm, in accordance with ASTM D257-99, and at least three measurements were conducted to obtain the average value. In order to accurately measure the resistivity, the sample surface was coated with a copper paste to ensure good electrical contact. For the nanocomposite samples subjected to alignment by the magnetic field, the resistivity was measured in both the perpendicular and parallel direction of the applied magnetic field.

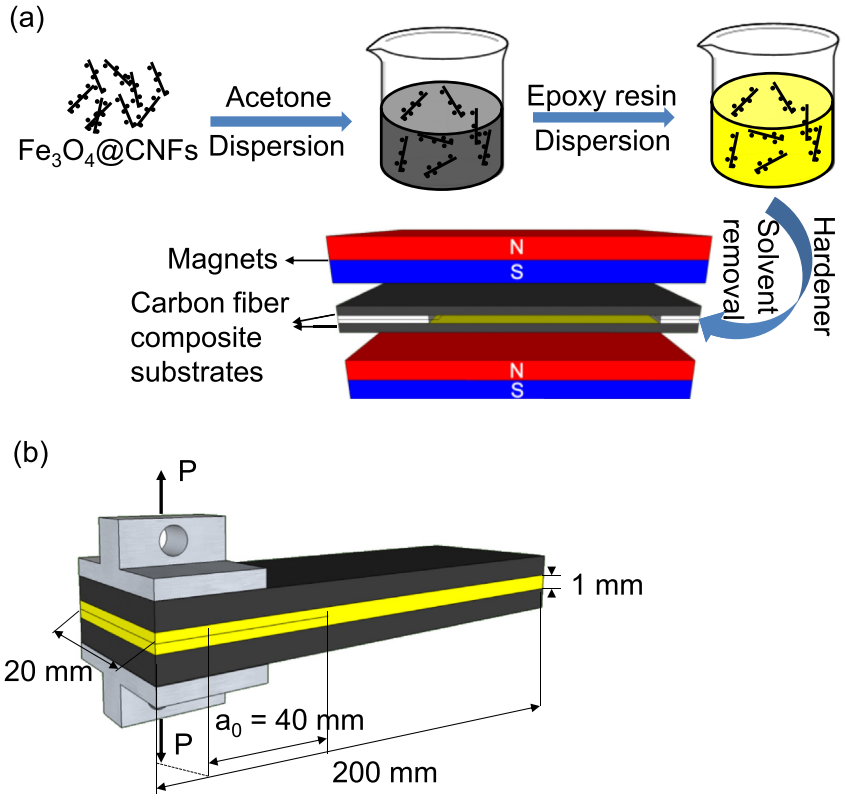

Fig. 1. Schematic of (a) composite joint preparation and (b) the DCB specimen, where a_0 is the initial crack length. The symbols N and S denote the magnetic poles of the permanent magnets.

The mode I fracture energy, G_{Ic}, of the epoxy nanocomposite layer was obtained from tests undertaken using the DCB bonded joints. A sharp crack tip was produced by carefully wedging the crack open from the tip of the inserted Teflon film. Load was applied to the specimens at a crosshead speed of 1 mm/min in accordance with ISO 25217. At least five replicate specimens were tested for each formulation. The crack growth was measured by using a travelling microscope. The mode I fracture energy was calculated based on "corrected beam theory" [34]. The crack was always found to propagate cohesively through the centre of the epoxy polymer layer, and thus the values of G_{Ic} could be readily ascertained.

3. Results and discussion

3.1. Characterization of the magnetic Fe_3O_4@CNFs

Fig. 2a and b shows the representative SEM images of the pristine CNFs and the Fe_3O_4@CNFs. The pristine CNFs show relatively smooth surfaces. By contrast, it can be clearly seen in Fig. 2b that there are some Fe_3O_4 nanoparticles (i.e. the bright domains) attached to the surfaces of the CNFs. It may be noted that the Fe_3O_4 nanoparticles are not covering the entire surface of the nanofibers and randomly distributed on the surface, but tend to form clusters. To further study the attachment of the Fe_3O_4 nanoparticles, TEM images were taken and are shown in Fig. 2c and d. These TEM images show that the clusters consist of small nanoparticles with an average diameter of 5–10 nm. The nanoparticles appear to be firmly anchored to the surface of the carbon nanofibers even after ultrasonication treatment. To verify the composition of the nanofiber hybrids, they were subjected to EDX analysis during the SEM investigation. Fig. 2e shows the EDX spectrum taken at the location indicated by the arrow in the inset image, confirming the presence of Fe and O elements. The magnetic nature of the as-prepared Fe_3O_4@CNFs was demonstrated by placing a magnet next to an ethanol dispersion of the nanofiber hybrids. The photograph on the left hand side in Fig. 2f shows the initial ethanol dispersion of Fe_3O_4@CNFs whilst the one on the right hand side shows its response to an external magnet placed next to it. The Fe_3O_4@CNFs were found to be attracted instantly to the external magnet.

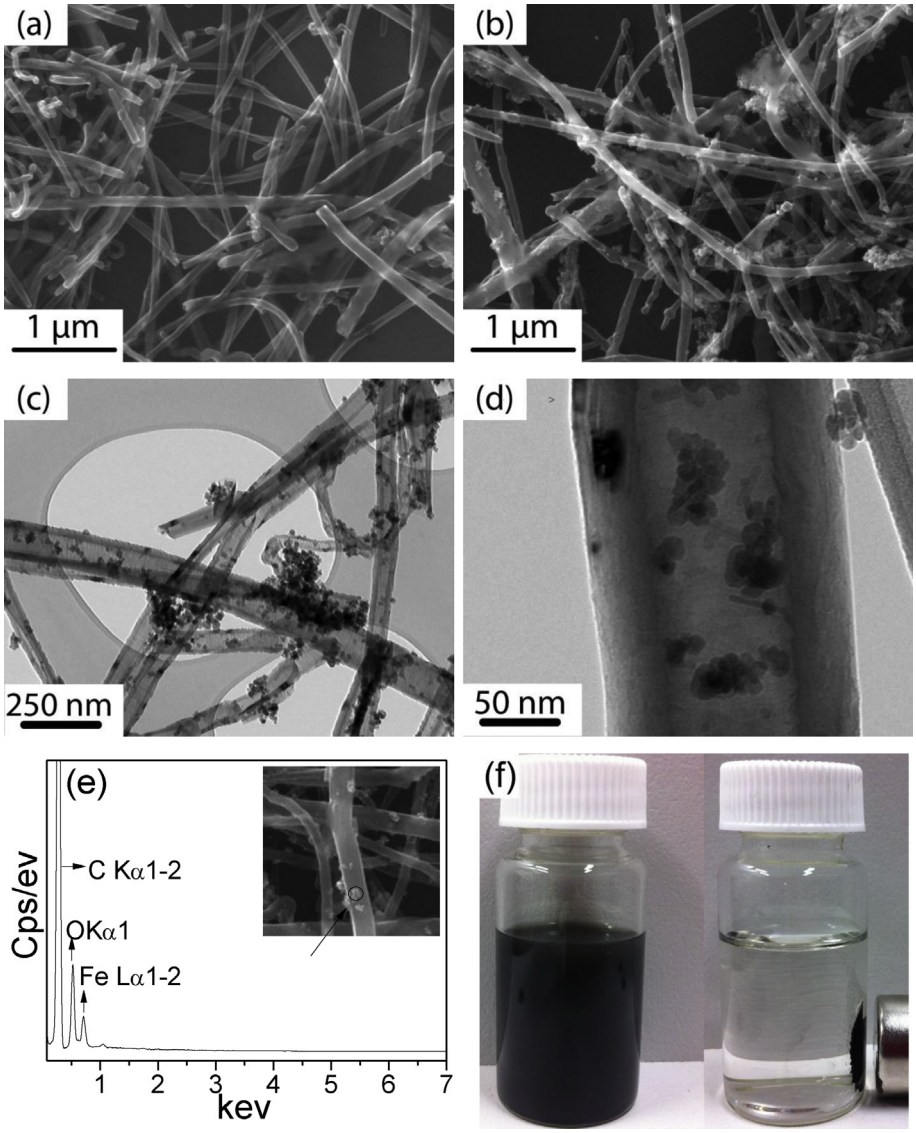

Fig. 2. SEM images of the (a) pristine CNFs and (b) Fe_3O_4@CNFs; (c) and (d) are TEM images of Fe_3O_4@CNFs at low and high magnification, respectively; (e) an EDX spectrum showing the elemental composition of the point indicated by a circle in the inserted SEM image in (e); and (f) shows the ferromagnetic behaviour of the Fe_3O_4@CNFs.

Fig. 3 shows the XRD patterns of the pristine CNFs, CNFs-OX, Fe_3O_4@CNFs, and iron oxide. The iron oxide was prepared following the same procedure as described in Section 2.2 but with the absence of the CNFs-OX for comparison. There is a sharp diffraction peak at 26.6° in the XRD spectrum of the CNFs which can be attributed to the (002) plane of their graphite structure [31]. After acid treatment, this sharp diffraction peak remains unchanged indicating that the crystalline structure of the CNFs has not been affected significantly. The main characteristic XRD peaks of iron oxide are located at 2θ = 30.4°, 35.7°, 43.2°, 53.6°, 57.3°, and 62.8° and they respectively correspond to the (220), (311), (400), (422), (511), and (440) planes of maghemite (γ-Fe_2O_3) and/or magnetite (Fe_3O_4) [35]. Maghemite and magnetite exhibit very similar XRD patterns and it is difficult to distinguish between these two phases [36]. Therefore, XPS (see Fig. 4) was employed to further verify the presence of the phase of the magnetic iron oxide. For the Fe_3O_4@CNFs, the characteristic XRD peaks of both CNFs and iron oxide can be clearly seen in the spectrum. The peak positions agree well with the diffraction peaks of both the iron oxide and the CNFs appearing at 2θ = 30.4°, 35.7°, 43.2°, 53.6°, 57.3°, 62.8°, and 26.6°.

XPS was used to study the surface chemistry of the Fe_3O_4@CNFs and the survey spectrum is given in Fig. 4a. For comparison, the survey spectra of the pristine CNFs and CNFs-OX are also provided. The typical asymmetric peak in the C1s region and symmetric peak in the O1s region can be seen in all the survey spectra of the CNFs, CNFs-OX, and Fe_3O_4@CNFs. The O1s/C1s peak area ratio increases for the CNFs-OX confirming the oxidization of the CNFs. The survey spectrum of the Fe_3O_4@CNFs indicates the presence of the elements Fe, O, and C.

To further characterize the chemical compositions and chemical oxidation states, high resolution XPS scans in the O1s, C1s, and Fe2p regions were recorded. Fig. 4b shows the O1s XPS spectra of the CNFs, CNFs-OX, and Fe_3O_4@CNFs, as well as the Fe2p scans of Fe_3O_4@CNFs. The O1s peaks of the CNFs are deconvoluted into three peaks: peak 1 at 532.0 eV corresponding to oxygen with a double bond to carbon (C═O) [37]; peak 2 at 533.1 eV corresponding to oxygen with a single bond to carbon (C–O) [31]; and peak 3 at 534.8 eV corresponding to oxygen atoms absorbed on the surface of the CNFs. Compared to the O1s spectra of the CNFs, the O1s spectra of the CNFs-OX show similar peaks but peak 1 shifts to 531.4 eV, which is likely due to the presence of more carbonyl groups on the surface after nitric acid oxidation. The relative content of carbonyl groups increases from 27.48% to 31.61%, providing further evidence of oxidation. For the Fe_3O_4@CNFs, an additional peak at 530.1 eV can be seen in the O1s spectrum revealing the presence of lattice oxygen in Fe_3O_4 [38]. From the Fe2p spectrum, the Fe2p1/2 and 2p3/2 peaks are observed at around 710.9 and 724.6 eV indicating the presence of a mixed oxide of Fe(II) and Fe(III), namely, Fe_3O_4 [38,39]. A very small shoulder exists at 719 eV, indicating the presence of a relatively small concentration of γ-Fe_2O_3.

The functionalisation of the CNFs with Fe_3O_4 was further confirmed by using FTIR spectroscopy (see Fig. 5). The pristine CNFs exhibit absorption bands at 1620 and 3440 cm^{-1} which can be assigned to the aromatic C═C [27] and H_2O adsorbed in the KBr disc [40], respectively. Compared to the pristine CNFs, the CNFs-OX were expected to show some new characteristic bands due to polar functional groups that have been introduced, including $\nu_{C=O}$ at ~1700 cm^{-1} and ν_{OH} at ~3400 cm^{-1} [32]. However, these characteristic bands cannot be clearly identified, probably due to the very low concentration of such functional groups. This was confirmed by the above XPS measurements which showed that the concentration of elemental oxygen in the CNFs-OX is 4.2%, which is slightly higher than that of the pristine CNFs (i.e. 3.4%). For the Fe_3O_4@CNFs, the absorption band observed at 597 cm^{-1} is associated with Fe–O–Fe stretching vibrations, which indicates the presence of magnetite nanoparticles [32].

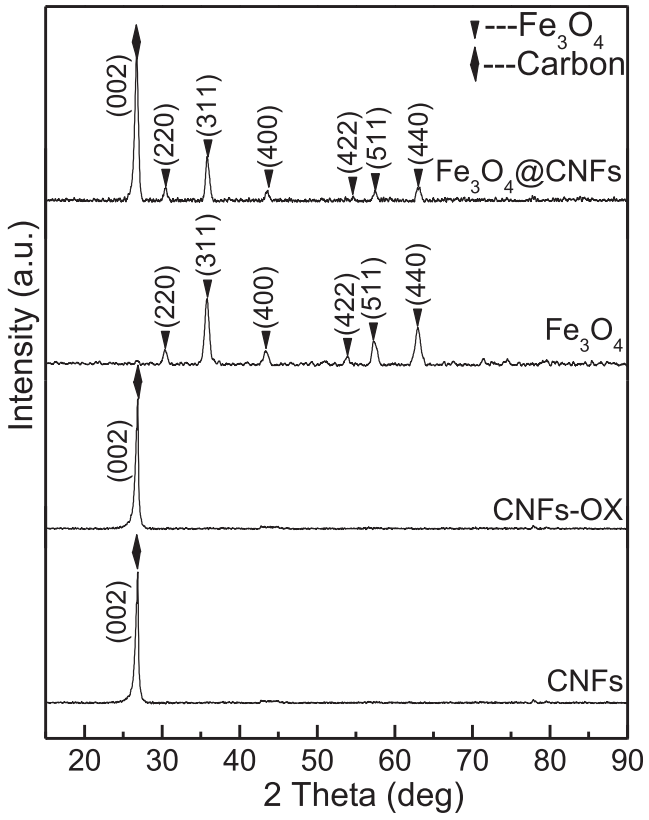

Fig. 3. XRD patterns of pristine CNFs, CNFs-OX, Fe_3O_4, and Fe_3O_4@CNFs.

3.2. Alignment of Fe_3O_4@CNFs in the epoxy nanocomposites

The alignment of the Fe_3O_4@CNFs in the liquid epoxy resin was observed using optical microscopy. Fig. 6a shows a typical optical micrograph of an epoxy resin that was not subjected to the external magnetic field. Clearly, the Fe_3O_4@CNFs are randomly-oriented in the epoxy resin. This micrograph also reveals that the nanofiber hybrids are well dispersed. Fig. 6b shows a typical optical micrograph of the liquid epoxy resin containing Fe_3O_4@CNFs subjected to the applied magnetic field. This micrograph confirms the alignment and chain-like structure of the nanofiber hybrids in the direction of the applied magnetic field, as indicated by the arrow. The alignment and chain-like structure of the Fe_3O_4@CNFs may be ascribed to the anisotropic nature of the dipolar interactions of the iron oxide nanoparticles close to the ends of the Fe_3O_4@CNFs [10,41]. Without an externally applied magnetic field, the magnetic moments of the iron oxide nanoparticles are randomly oriented leading to vanishing net magnetization. However, upon the application of a sufficiently large magnetic field, the magnetic moments of the nanoparticles align along the external field direction and the resultant dipolar interactions orient the Fe_3O_4@CNFs. Attraction of the north and south poles of the magnetic carbon nanofibers resulted in the formation of the chain-like structure.

After the epoxy was cured, the microstructures of the epoxy nanocomposites were examined by SEM and TEM to ascertain whether the aligned structure achieved while the epoxy was liquid remained in place. For comparison, Fig. 6c shows a SEM image of the epoxy nanocomposite without being subjected to any applied

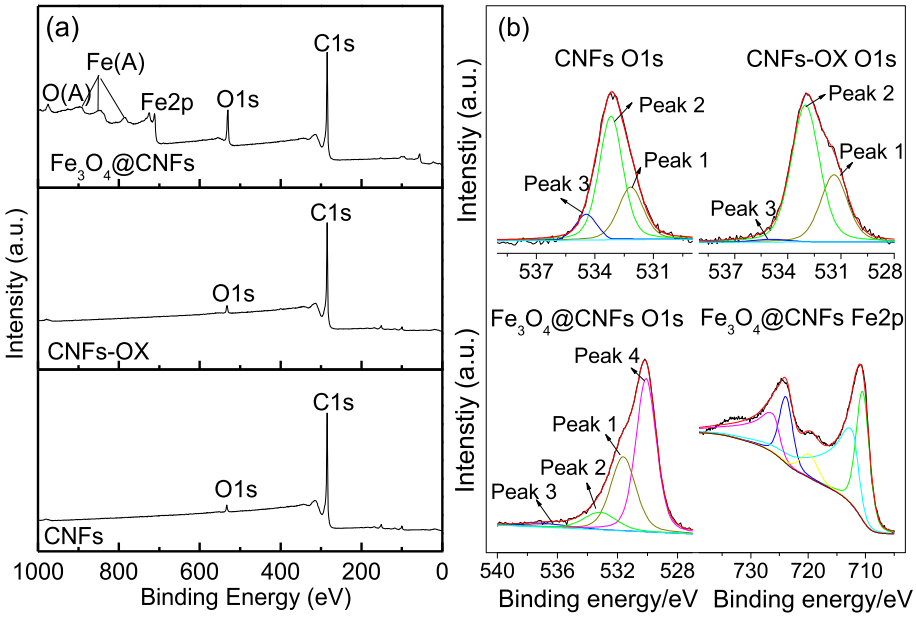

Fig. 4. XPS spectra: (a) survey spectrum of pristine CNFs, CNFs-OX, and Fe_3O_4@CNFs; (b) high resolution O1s and Fe2p scans of CNFs, CNFs-OX, and Fe_3O_4@CNFs.

magnetic field. As expected, the Fe_3O_4@CNFs (i.e. the bright spots) are uniformly dispersed and randomly-oriented in the epoxy polymer (i.e. the grey continuous area). For the epoxy nanocomposites subjected to the magnetic field during curing, Fig. 6d reveals that the Fe_3O_4@CNFs are aligned parallel to the direction of the magnetic field, consistent with the observed alignment in the liquid epoxy resin prior to cure (see Fig. 6b). The TEM images (see Fig. 6e and f) further support the above conclusions on the orientation of the nanofiber hybrids, parallel to the applied magnetic field, in the epoxy nanocomposites.

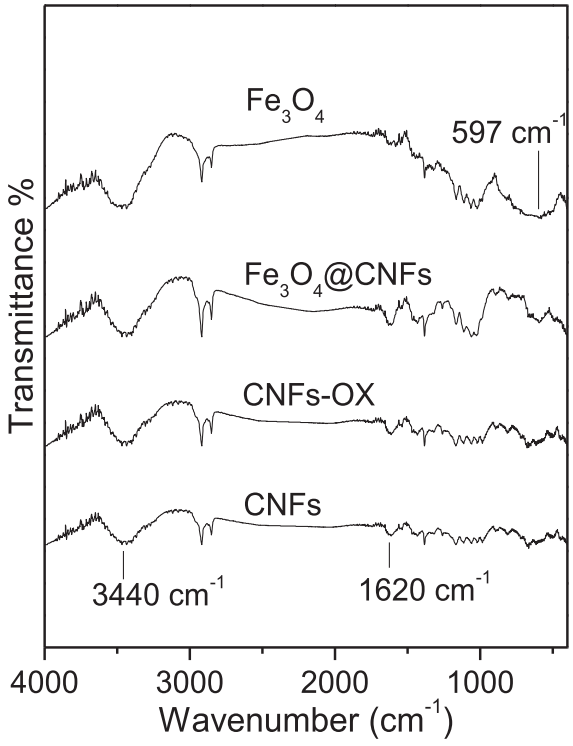

Fig. 5. FTIR spectra of pristine CNFs, CNFs-OX, Fe_3O_4@CNFs, and Fe_3O_4.

3.3. Electrical conductivity studies

Fig. 7 shows the conductivity of the epoxy nanocomposites with different contents of randomly-oriented and aligned Fe_3O_4@CNFs. The electrical conductivities of the Fe_3O_4@CNFs epoxy nanocomposites subjected to the magnetic field were measured in two directions, namely, parallel and perpendicular to the direction of the externally applied magnetic field. The unmodified epoxy exhibits a conductivity of ~10^{-13} S/m which increases to ~10^{-12} S/m and ~10^{-10} S/m for the epoxy nanocomposites containing 0.2 wt% and 0.6 wt% of randomly-oriented Fe_3O_4@CNFs, respectively. For the epoxy nanocomposites cured under the applied magnetic field, a higher electrical conductivity is observed when measured in the direction parallel to the magnetic field. Indeed, the conductivity in the direction parallel to the magnetic field is consistently over one order of magnitude higher than that for the nanocomposites containing randomly-oriented Fe_3O_4@CNFs. This is similar to the reported increase from the use of CNTs aligned by a magnetic field of 25 T [42,43]. By contrast, the electrical conductivity measured normal to the magnetic field shows no significant increase compared to the nanocomposites containing randomly-oriented Fe_3O_4@CNFs. This demonstrates that the application of the magnetic field leads to the resultant epoxy nanocomposites possessing anisotropic electrical properties. However, the improvement of the electrical conductivities was not that remarkable. It has been reported that higher the oxygen concentration present in the CNFs, then higher is the content of CNFs required to reach the percolation threshold [44]. During the preparation of the Fe_3O_4@CNFs, a strong acid was employed to treat the CNFs, which might have introduced some defects and some oxidative surface groups. This partially may account for the relatively low electrical conductivity of the epoxy nanocomposites. Additionally, coating the surface of CNFs with iron oxide nanoparticles, which have a relatively high resistivity, would further reduce the electrical conductivity of the nanocomposite [10,25].

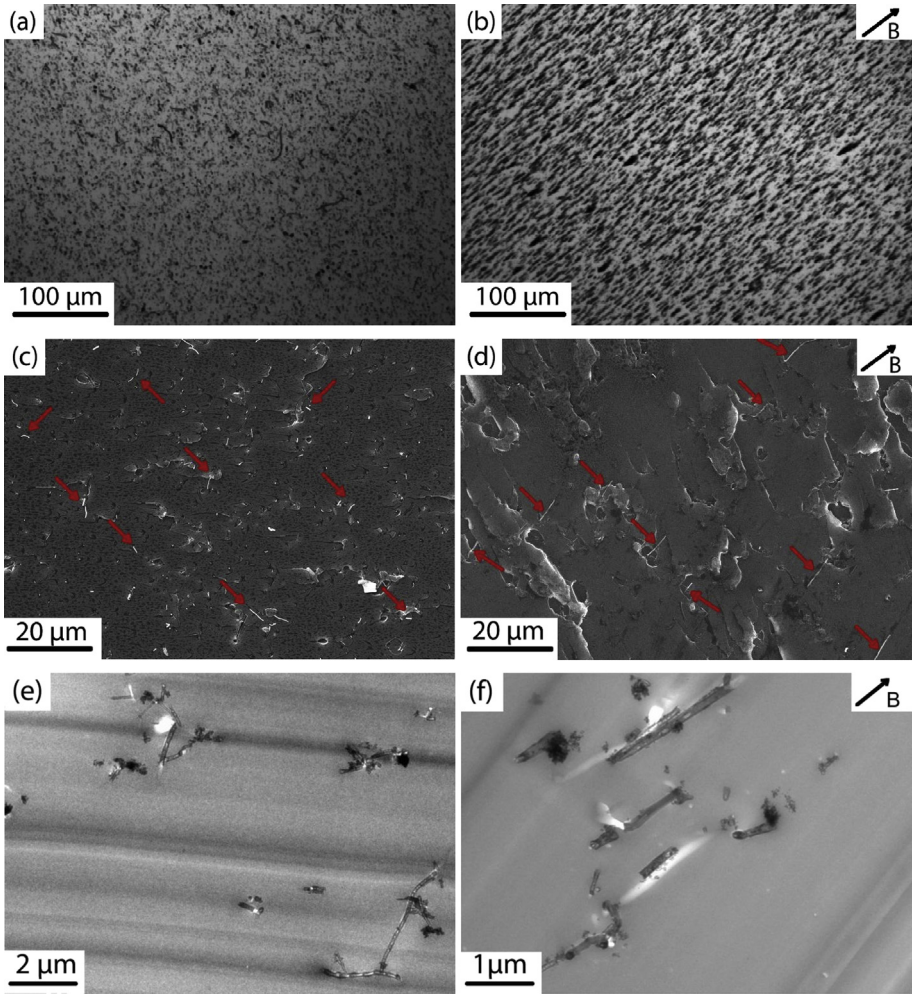

Fig. 6. Representative optical micrographs (a and b), SEM images (c and d), and TEM (e and f) images of epoxy nanocomposites containing 0.6 wt% of randomly-oriented Fe_3O_4@CNFs (i.e. (a), (c), and (e)) and Fe_3O_4@CNFs aligned under the 50 mT magnetic field (i.e. (b), (d), and (f)). The black arrows in (b), (d), and (f) indicate the direction of the applied magnetic field (B). The red arrows in (c) and (d) indicate the nanofiber hybrids. (For interpretation of the references to colour in this figure legend, the reader is referred to the web version of this article.)

3.4. Fracture toughness studies

The effects of the alignment of the nanofiber hybrids on the fracture toughness of the epoxy nanocomposites were studied by investigating the mode I fracture behaviour of the carbon fiber composite joints bonded using the epoxy nanocomposites (or the unmodified epoxy polymer). The unmodified epoxy polymer and all the epoxy nanocomposites exhibited unstable, stick-slip, crack growth behaviour. Such behaviour gives rise to classic 'saw-tooth' shaped load versus displacement curves. Fig. 8a shows the typical load versus displacement curves for an epoxy nanocomposite containing 0.6 wt% of Fe_3O_4@CNFs. The maximum load values are associated with the onset of crack growth, which is followed by very rapid crack growth leading to the crack arresting at the lower load values. Following ISO 25217, the value of the fracture energy, G_{Ic}, for the onset of crack growth was determined using the maximum load values. Fig. 8b presents the values of G_{Ic} of the unmodified epoxy polymer and the epoxy nanocomposites containing either randomly-oriented or aligned nanofiber hybrids. The average fracture energy of the unmodified epoxy polymer is 134 J/m^2. With the addition of 0.4 wt% of randomly-oriented nanofiber hybrids, the fracture energy increased to 242 J/m^2. The application of the external magnetic field, which oriented the Fe_3O_4@CNFs in a direction normal to the crack surface, further improved the fracture energy to 328 J/m^2. It can be seen from Fig. 8b that increasing the content of the Fe_3O_4@CNFs beyond 0.4 wt% did not yield any further significant improvements in G_{Ic} of the epoxy nanocomposites containing either the randomly-oriented or aligned nanofiber hybrids.

3.5. Toughening mechanisms

To identify the toughening mechanisms, the fracture surfaces of the unmodified epoxy polymer and epoxy nanocomposites from the DCB tests were examined, both visually and using the SEM. From a visual inspection, for both the unmodified epoxy polymer and epoxy nanocomposites, there were distinct 'thumbnail lines' on the fracture surfaces where the onset of crack propagation and then crack arrest had occurred. Further, for the epoxy nanocomposites, stress-whitening was observed along the 'thumbnail lines' which indicated the occurrence of more extensive damage at the crack tip prior to crack propagation in the nanocomposites compared to the unmodified epoxy polymer. Such an observation is typically associated with an enhanced toughness.

Fig. 9a shows SEM images of the fracture surfaces of the DCB specimens bonded using the unmodified epoxy polymer. The

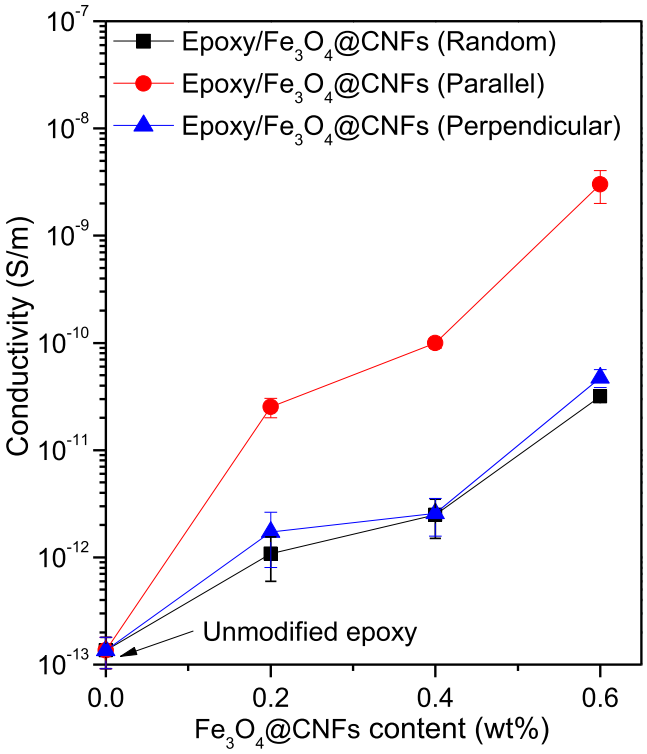

Fig. 7. Electrical conductivity of the epoxy nanocomposites containing 0.0, 0.2, 0.4, and 0.6 wt% of Fe_3O_4@CNFs. (The orientation of the Fe_3O_4@CNFs with respect to the direction of measurement is indicated.)

fracture surface is very smooth and featureless, indicating a very brittle fracture behaviour. On the other hand, the presence of Fe_3O_4@CNFs in the epoxy produced much rougher surfaces and patterns of tear marks, as shown in Fig. 9b–d. These are likely to arise from crack deflection due to the presence of the Fe_3O_4@CNFs and plastic deformation of the epoxy polymer surrounding the Fe_3O_4@CNFs. A closer inspection of the fracture surfaces reveals that the Fe_3O_4@CNFs were pulled out after debonding from the epoxy polymer, with some Fe_3O_4@CNFs being peeled away from the epoxy (see Fig. 9b–d). Cavities and grooves created by the pull-out and debonding of the Fe_3O_4@CNFs, as well as ruptured Fe_3O_4@CNFs, are evident in Fig. 9d and e. A high magnification SEM image (see Fig. 9e) reveals that there are voids surrounding the Fe_3O_4@CNFs. These voids are typically created due to debonding of the Fe_3O_4@CNFs from the epoxy polymer, followed by plastic deformation of the epoxy. This plastic void growth mechanism will also absorb energy and will further enhance the fracture energy of the nanocomposites. Behind the advancing crack tip, Fe_3O_4@CNFs are pulled out from the epoxy polymer and bridge the crack faces, as shown by a cross-section image in Fig. 10. The alignment of the Fe_3O_4@CNFs in the direction normal to the crack surface increases the possibility of such interactions between the advancing crack tip and the Fe_3O_4@CNFs.

Similar toughening mechanisms to those described above have been reported for epoxy nanocomposites containing MWCNTs [45] and all of these toughening mechanisms contribute to the measured increases in the fracture energy, G_{Ic}, for the epoxy nanocomposites. The nanocomposites containing nanofiber hybrids aligned normal to the crack surface are more effective at inducing such toughening mechanisms than those containing only randomly-oriented nanofiber hybrids, leading to a significantly higher G_{Ic}.

4. Conclusions

Fe_3O_4@CNFs hybrids have been fabricated by attaching magnetite nanoparticles to CNFs through a simple and effective co-precipitation method. Using the techniques of optical microscopy, SEM and TEM, it has been conclusively established that the Fe_3O_4@CNFs can be aligned in the liquid epoxy resin by the application of a relatively weak magnetic field (~50 mT), and that this alignment of the nanofiber hybrids is maintained after the epoxy nanocomposites are cured. Compared to the unmodified epoxy polymer, the epoxy nanocomposites exhibit a higher electrical conductivity, especially along the direction of the alignment. In addition, alignment of the Fe_3O_4@CNFs significantly improves the toughening efficiency. For example, the addition of 0.4 wt% of aligned Fe_3O_4@CNFs increases the fracture energy of the epoxy nanocomposites by about 150% above that of the unmodified epoxy polymer. By contrast, randomly-oriented Fe_3O_4@CNFs at the same

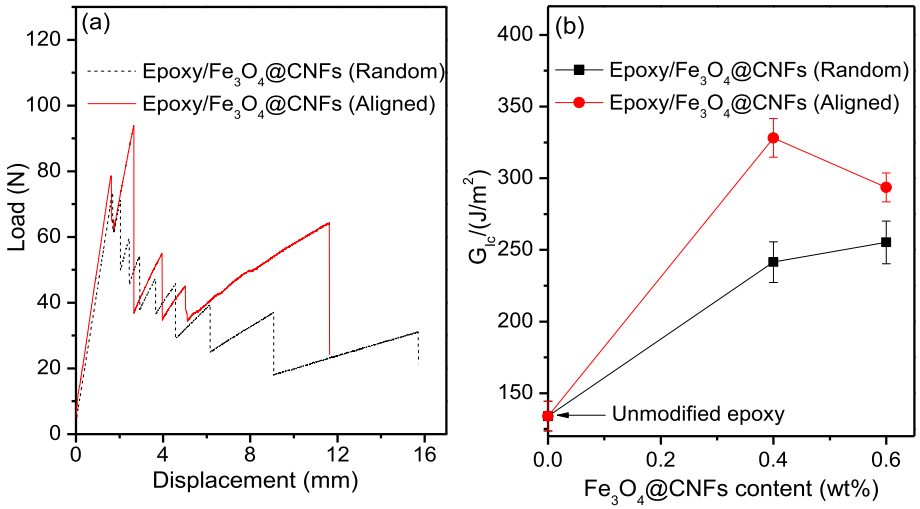

Fig. 8. (a) Representative load versus displacement curves of the epoxy nanocomposites with 0.6 wt% of randomly-oriented or aligned Fe_3O_4@CNFs; (b) the mode I fracture energy, G_{Ic}, of the epoxy nanocomposites as a function of the content of Fe_3O_4@CNFs. (The orientation of the Fe_3O_4@CNFs was either random or aligned normal to the crack surface, as indicated.)

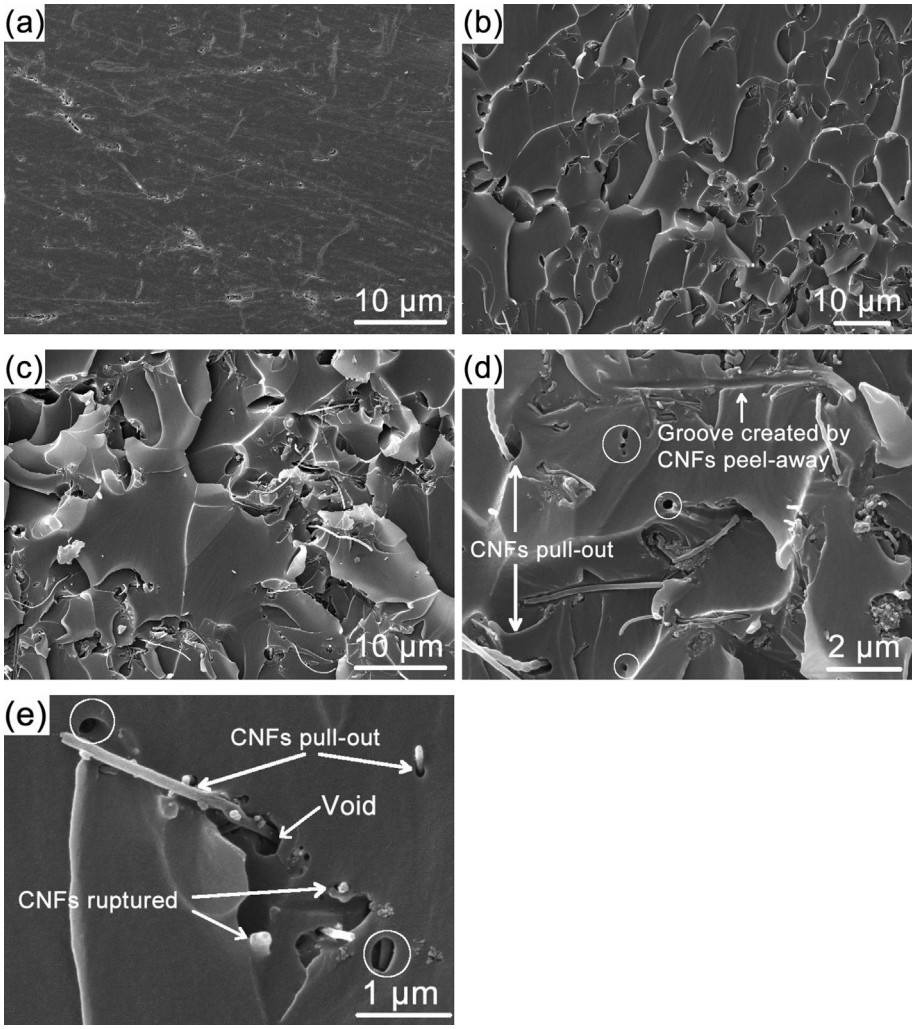

Fig. 9. SEM micrographs of the fracture surfaces of (a) the unmodified epoxy polymer and (b–e) the epoxy nanocomposites containing 0.6 wt% of aligned Fe_3O_4@CNFs. The white circles in (d) and (e) indicate the cavities created by pull-out of the Fe_3O_4@CNFs.

content only give about an 80% improvement. Based on fractographic analyses, the main toughening mechanisms induced by the nanofiber hybrids include interfacial debonding, pull-out, crack bridging and rupture of the Fe_3O_4@CNFs, and plastic void growth in the epoxy polymer. The alignment of the Fe_3O_4@CNFs in the direction normal to the crack surface increases their propensity to interact with the advancing crack tip, leading to more effective toughening. The present work has clearly demonstrated that by attaching magnetite nanoparticles to CNFs the resulting nanofiber hybrids can be aligned in an epoxy polymer using a relatively weak magnetic field. The epoxy nanocomposites so produced exhibit significant improvements in their electrical conductivity and fracture toughness.

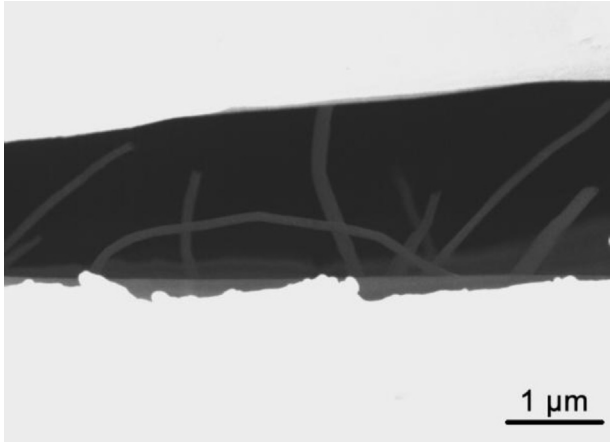

Fig. 10. SEM micrograph of the cross-section (i.e. side view) of the crack tip of a DCB specimen bonded with the epoxy nanocomposites containing 0.6 wt% of aligned Fe_3O_4@CNFs.

Acknowledgements

The authors are thankful for the financial support received from the Australian Research Council's Discovery Grant (DP140100778).

References

[1] Jia JJ, Sun XY, Lin XY, Shen X, Mai YW, Kim JK. ACS Nano 2014;8:5774–83.
[2] Meng QS, Jin J, Wang RY, Kuan HC, Ma J, Kawashima N, et al. Nanotechnology 2014;25:125707.
[3] Roy S, Das T, Zhang L, Li Y, Ming Y, Ting S, et al. Polymer 2015;58:153–61.
[4] Ma HY, Chen XM, Hsiao BS, Chu B. Polymer 2014;55:160–5.
[5] Al-Saleh MH, Sundararaj U. Polymer 2010;51:2740–7.
[6] Liao K-H, Qian Y, Macosko CW. Polymer 2012;53:3756–61.
[7] Park YT, Qian Y, Chan C, Suh T, Nejhad MG, Macosko CW, et al. Adv Funct Mater 2014:575–85.

[8] Vennerberg D, Hall R, Kessler MR. Polymer 2014;55:4156–63.
[9] Ajayan PM, Stephan O, Colliex C, Trauth D. Science 1994;265:1212–4.
[10] Kim IT, Tannenbaum A, Tannenbaum R. Carbon 2011;49:54–61.
[11] Yousefi N, Gudarzi MM, Zheng Q, Lin X, Shen X, Jia J, et al. Compos Part A 2013;49:42–50.
[12] Yousefi N, Sun X, Lin X, Shen X, Jia J, Zhang B, et al. Adv Mater 2014;26:5480–7.
[13] Yousefi N, Lin X, Zheng Q, Shen X, Pothnis JR, Jia J, et al. Carbon 2013;59:406–17.
[14] Wang Q, Dai JF, Li WX, Wei ZQ, Jiang JL. Compos Sci Technol 2008;68:1644–8.
[15] Bradford PD, Wang X, Zhao HB, Maria JP, Jia QX, Zhu YT. Compos Sci Technol 2010;70:1980–5.
[16] Schwarz M-K, Bauhofer W, Schulte K. Polymer 2002;43:3079–82.
[17] Martin CA, Sandler JKW, Windle AH, Schwarz MK, Bauhofer W, Schulte K, et al. Polymer 2005;46:877–86.
[18] Steinert BW, Dean DR. Polymer 2009;50:898–904.
[19] Abdalla M, Dean D, Theodore M, Fielding J, Nyairo E, Price G. Polymer 2010;51:1614–20.
[20] Mahfuz H, Zainuddin S, Parker M, Al-Saadi T, Rangari V, Jeelani S. J Mater Sci 2009;44:1113–20.
[21] Camponeschi E, Vance R, Al-Haik M, Garmestani H, Tannenbaum R. Carbon 2007;45:2037–46.
[22] Shi D, He P, Lian J, Chaud X, Bud'ko SL, Beaugnon E, et al. J Appl Phys 2005;97:064312.
[23] Fragouli D, Das A, Innocenti C, Guttikonda Y, Rahman S, Liu L, et al. ACS Appl Mater Interfaces 2014;6:4535–41.
[24] Malkina O, Mahfuz H, Sorge K, Rondinone A, Chen J, More K, et al. AIP Adv 2013;3:042104.
[25] Prolongo SG, Meliton BG, Del Rosario G, Urena A. Compos Part B 2013;46:166–72.
[26] Yan HY, Tang YX, Long W, Li YF. J Mater Sci 2014;49:5256–64.
[27] Jiao WC, Shioya M, Wang RG, Yang F, Hao LF, Niu Y, et al. Compos Sci Technol 2014;99:124–30.
[28] Al-Saleh MH, Sundararaj U. Carbon 2009;47:2–22.
[29] Ren T, Si Y, Yang JM, Ding B, Yang XX, Hong F, et al. J Mater Chem 2012;22:15919–27.
[30] Si Y, Ren T, Ding B, Yu J, Sun G. J Mater Chem 2012;22:4619–22.
[31] Zhong RS, Qin YH, Niu DF, Zhang XS, Zhou XG, Sun SG, et al. Electrochim Acta 2013;89:157–62.
[32] Cunha C, Panseri S, Iannazzo D, Piperno A, Pistone A, Fazio M, et al. Nanotechnology 2012;23:465102.
[33] Zhang J, Wang JF, Lin T, Wang CH, Ghorbani K, Fang J, et al. Chem Eng J 2014;237:462–8.
[34] Blackman BRK, Kinloch AJ. Fracture tests on structural adhesive joints. In: Moore APDR, Williams JG, editors. European Structural Integrity Society. Elsevier; 2001. p. 225–67.
[35] Kim IT, Nunnery GA, Jacob K, Schwartz J, Liu XT, Tannenbaum R. J Phys Chem C 2010;114:6944–51.
[36] Sun Z, Liu Z, Wang Y, Han B, Du J, Zhang J. J Mater Chem 2005;15:4497–501.
[37] Cuervo MR, Asedegbega-Nieto E, Díaz E, Vega A, Ordóñez S, Castillejos-López E, et al. J Chromatogr A 2008;1188:264–73.
[38] Bhuvaneswari S, Pratheeksha PM, Anandan S, Rangappa D, Gopalan R, Rao TN. Phys Chem Chem Phys 2014;16:5284–94.
[39] Zhu S, Guo J, Dong J, Cui Z, Lu T, Zhu C, et al. Ultrason Sonochem 2013;20:872–80.
[40] Zhou J-H, Sui Z-J, Zhu J, Li P, Chen D, Dai Y-C, et al. Carbon 2007;45:785–96.
[41] Correa-Duarte MA, Grzelczak M, Salgueirino-Maceira V, Giersig M, Liz-Marzan LM, Farle M, et al. J Phys Chem B 2005;109:19060–3.
[42] Choi ES, Brooks JS, Eaton DL, Al-Haik MS, Hussaini MY, Garmestani H, et al. J Appl Phys 2003;94:6034–9.
[43] Kimura T, Ago H, Tobita M, Ohshima S, Kyotani M, Yumura M. Adv Mater 2002;14:1380–3.
[44] Lim CS, Rodriguez AJ, Guzman ME, Schaefer JD, Minaie B. Carbon 2011;49:1873–83.
[45] Hsieh TH, Kinloch AJ, Taylor AC, Kinloch IA. J Mater Sci 2011;46:7525–35.